

# A New Orientation Indicator for Radio-Quiet Quasars

Todd A. Boroson

*National Optical Astronomy Observatory<sup>1</sup>, P.O. Box 26732, Tucson, AZ 85726*

## ABSTRACT

The velocities of the [O III]  $\lambda 5007$  and optical Fe II emission lines, measured relative to the systemic redshifts of 2265 QSOs by Hu et al. (2008), show the signature of a disklike BLR structure with polar outflows. Objects with large [O III] outflows show no Fe II offset velocity and are seen pole-on. Objects with large Fe II inflow show no [O III] offset velocity and are seen edge-on. This interpretation is supported by the morphology of the radio-loud objects within the sample and by previous determinations of the geometry of the broad and narrow line regions. Analysis of the objects with neither Fe II or [O III] velocity offsets, however, show that the two groups also differ in Eddington ratio, and, within this subset, corresponding groups with high and low Eddington ratio but with the opposite orientation can be identified.

Using these four subsets of the sample, the effects of orientation and Eddington ratio can be separated, and, in some cases, quantified. The changes in apparent continuum luminosity and broad  $H\beta$  width and strength suggest a model in which both continuum and  $H\beta$  are emitted from the surface of the disk, which is less flattened in high Eddington ratio objects. The effects of orientation on the derived properties, black hole mass and Eddington ratio, are significant, though not large. The [O III] outflow appears to influence the width of that line, as well as its centroid.

*Subject headings:* quasars: emission lines — quasars: general — black hole physics

## 1. Introduction

It has long been recognized that AGN are not spherical. Angular momentum of the fueling material implies the development of a disk. Radio jets are obviously bipolar. The obscuring material that drives the Type 1-Type 2 dichotomy is thought to be toroidal. In nearby objects, the narrow line region (NLR) is often seen to be biconical.

However, the compelling case for a quantitative orientation indicator has been problematic. In radio-loud objects, it is believed that the degree of radio core dominance is indicative of the orientation, in that bright cores represent the doppler-enhanced emission from viewing close to the axis of the jet (Blandford & Konigl 1979; Wills & Browne 1986). Radio-loud objects repre-

sent a small fraction of AGN, though, and even within this fraction, the intrinsic radio properties vary with radio luminosity. Thus, the identification of large samples of objects that are identical other than orientation is not straightforward.

For radio-quiet objects, the recent availability of very large and relatively complete samples of AGN from the Sloan Digital Sky Survey (SDSS) (York et al. 2000) make a statistical approach possible for the first time. While studies of samples of tens or hundreds of objects (Boroson & Green 1992; Marziani et al. 2003) have discerned patterns and correlations in the observed properties of QSOs, an understanding of how to identify and separate the effects of the overall drivers – both physical and geometrical – requires much larger samples. Important steps in this direction have been taken by studies such as Richards et al. (2002), Hu et al. (2008), Risaliti et al. (2011), and Decarli et al. (2011), all of whom find evidence for orientation effects among the properties that they

<sup>1</sup>The National Optical Astronomy Observatory is operated by AURA, Inc., under cooperative agreement with the National Science Foundation.

investigated. None of these studies, however, have produced a general technique for determining the orientation of a given object, or for identifying subsets of analogous objects differing only by orientation.

Despite the lack of an unambiguous orientation indicator, a picture of the geometric structure of active nuclei has emerged (Urry & Padovani 1995; Gaskell 2009; Crenshaw et al. 2010). The region that emits the lower ionization broad lines is thought to be somewhat disklike. Material in this disk may be flowing inwards, but there may also be rotation and turbulence. The optical continuum may also be emitted from a disk, interior to the broad line region (BLR). These disks are assumed to be coplanar with the dusty torus that obscures our view of the continuum and BLR in Type 2 objects. The higher ionization narrow lines are believed to arise in a biconical region that is perpendicular to the disk and flowing outward. Some fraction of the higher ionization broad lines may also participate in this polar outflow. The lower ionization narrow lines probably arise over a very large region dominated by the potential of the host galaxy rather than the central black hole.

In section 2, a diagram is constructed showing the relationship between the motions of the material that emits broad Fe II and that which emits narrow [O III]. This diagram is most obviously interpreted as indicating the orientation of two groups of quasars, one pole-on and one edge-on, within the general picture described above. Exploration of intermediate objects show that another factor, in addition to orientation, is at work; this is identified as  $L_{bol}/L_{Edd}$  or Eddington ratio (ER). These intermediate objects can be separated into subsets that match the pole-on and edge-on subsets in ER, but differ in orientation. Section 3 presents the characteristic properties of each of these four subsets, allowing a separation of the effects of the two factors. Finally, section 4 discusses the implications of the orientation-driven effects for determinations of black hole mass ( $M_{BH}$ ) and ER. Section 4 concludes with some questions that could be answered by further development of this technique.

## 2. The $V_{[OIII]}$ vs. $V_{FeII}$ Diagram

The study by Hu et al. (2008) was aimed at understanding the properties of Fe II emission in quasars. They decomposed the spectra of 4037  $z < 0.8$  quasars into continuum and multiple line contributions. These authors measure luminosity, width, and velocity shift parameters for  $H\beta$  (broad and narrow separately), [O III]  $\lambda 5007$ , Mg II  $\lambda 2800$ , and [O II]  $\lambda 3727$ . Because of the range of redshift covered, the Mg II and [O II] lines are only measured in a subset of the full sample. They also measure these parameters for the ensemble of Fe II lines in the range  $\lambda\lambda 4434-4684$ . They devote considerable effort to testing and demonstrating the accuracy of their technique - in particular, the velocity shifts.

Their sample is drawn from the SDSS DR5 (Adelman-McCarthy et al. 2007) quasar catalog (Schneider et al. 2007) with the following additional restrictions. They attempt to fit only objects having signal-to-noise ratio (S/N)  $> 10$  in the range  $\lambda\lambda 4430-5550$ . They then discard objects with poor fits to their model or with equivalent width of the Fe II emission ( $EW_{FeII}$ )  $< 25\text{\AA}$ . Finally, they discard objects with large errors in either the width of the broad  $H\beta$  or the velocity shift of [O III]  $\lambda 5007$ . These restrictions, particularly the minimum  $EW_{FeII}$ , should be kept in mind for statistical conclusions drawn from their sample.

Hu et al. (2008) adopt the [O III]  $\lambda 5007$  line to define the systemic redshift because they can measure its position in all objects in their sample. However,  $\lambda 5007$  is known to be blueshifted or to have excess emission on its blue wing in many objects (Zamanov et al. 2002; Boroson 2005). Shifts as large as several hundred  $\text{km s}^{-1}$  are occasionally seen. For this study, all the velocities have been renormalized to the [O II]  $\lambda 3727$  line, which is measured in 2265 of the objects. Objects without a measurement of velocity shift for [O II] were discarded.

Figure 1 shows the [O III] velocity shift plotted against the Fe II velocity shift for the 2265 objects. The random errors on the Fe II velocity shifts are about  $100 \text{ km s}^{-1}$  for small shifts and rise to about  $300 \text{ km s}^{-1}$  for the shifts of  $3000 \text{ km s}^{-1}$ . The errors on the [O III] velocity shifts are about  $25 \text{ km s}^{-1}$  for small shifts and rise to about

50 km s<sup>-1</sup> for the largest blueshifts, 700 km s<sup>-1</sup>. While the density of objects is highest around the origin, two tails are clearly seen. About 37% of the objects show almost no [O III] velocity shift, but significant Fe II redshift. About 10% of the objects show almost no Fe II velocity shift, but significant [O III] blueshift.

## 2.1. Effects of Orientation

Hu et al. (2008) argue that the Fe II redshift is caused by infall of material in the outer part of the BLR. They find that the Fe II lines are uniformly narrower than H $\beta$  and that the objects with large Fe II redshifts show excess emission on the red side of the H $\beta$  line. They also find that the Fe II redshifts are inversely correlated with ER. They speculate that the Fe II infall is driven by gravity and opposed by radiation pressure. The rise in radiation pressure with increasing ER decreases the inflow.

There is direct evidence supporting the idea that the blueshift of [O III] is indicative of a polar outflow. Studies of very nearby objects (Ruiz et al. 2005; Crenshaw et al. 2010) are able to resolve the NLR sufficiently to map the spatial and kinematic distribution of emitting material and match it to models of outflowing material and a biconical illumination pattern.

In light of these explanations of the velocities of the Fe II and [O III] emitting material, the obvious conclusion is that the tails in the  $v_{[OIII]}$  vs.  $v_{FeII}$  diagram are indicative of orthogonal motions - Fe II in the disk and [O III] in the perpendicular polar direction. In this case, the objects with large Fe II inflow velocities are seen with the disk edge-on to our line of sight, and the objects with large [O III] outflow velocities are seen with the disk pole-on to our line of sight. Therefore, we define three regions, shown in figure 1 as pole-on and edge-on subsets, and a third subset that includes objects with neither large Fe II velocities nor large [O III] velocities. The boundaries of these regions are arbitrary; they merely serve to isolate the two tails of the distribution. These boundaries result in 829 edge-on objects, 226 pole-on objects, and 1081 intermediate objects. Note that the term edge-on is used in a relative sense; an obscuring torus in the same plane as the Fe II emitting disk would limit actual viewing angles to be outside of a true edge-on value.

Some confirmation that this explanation is correct comes from the radio-loud objects in the sample. Within the edge-on subset, there are 778 objects within the footprint of the FIRST radio survey (Becker et al. 1995). A search of the FIRST archive at these positions yielded 59 objects with  $R > 10$ , where  $R$  is the ratio of 6 cm to 2500 Å flux. The FIRST images of each of these matches was inspected visually and classified as core, extended or resolved single source, core plus lobe, core plus 2 lobes, or 2 lobes with no core. Thirty of these edge-on objects are not compact radio sources, and of these, 17 show two lobes. Similarly, the pole-on subset was analyzed. Within that smaller subset, there are 7 radio-loud objects, of which 5 are compact, one is a resolved single source, and one has a core plus one lobe morphology. Assuming that the radio source axis is aligned with the [O III] outflow direction, this is as expected; double lobed objects are only seen within the edge-on subset. The intermediate subset shows intermediate radio properties; of the 40 objects in this subset that are radio-loud, five show two lobes. However, note that the radio-loud fraction of all these subsets is small, and the sample-wide characteristics apply to the radio-quiet objects as well.

## 2.2. Effects of Eddington Ratio

The argument that the tails in figure 1 isolate pole-on and edge-on subsets does not preclude the possibility that other factors play a role. One that should certainly be considered is  $L_{bol}/L_{Edd}$ , or Eddington ratio. Many trends in AGN characteristics, and, in particular, both of the effects that contribute to the  $v_{[OIII]}$  vs.  $v_{FeII}$  diagram have been related to Eddington ratio. Hu et al. (2008) argued that as Eddington ratio increases, radiation pressure opposes and eventually prevents the Fe II inflow. Similarly, Boroson (2005) and Zamanov et al. (2002) both find correlations between the objects with largest [O III] blueshifts and Eddington ratio. More generally, Eddington ratio has been proposed as a driver for the EV1 correlations (Boroson & Green 1992), which include FWHM of H $\beta$  and EW of both Fe II and [O III].

We begin with the hypothesis that the sequence of objects in the  $v_{[OIII]}$  vs.  $v_{FeII}$  diagram is due only to orientation. As one's viewing angle changes from edge-on to pole-on and passing

through an intermediate range, the Fe II inflow velocity becomes apparently smaller, while the [O III] outflow velocity becomes apparently larger. Within the intermediate range, objects show neither motion strongly and cluster around the origin. If orientation were the only factor, then properties of the objects near the origin should be intermediate between the two tails. Furthermore, relationships among those properties should behave in a way that tracks the relationships between the two tails.

The orientation-only hypothesis is disproven by figure 2, which shows the luminosity at  $\lambda 5100$  plotted against the FWHM of  $H\beta$  for the objects that have no significant offset velocity in either Fe II or [O III]. While the edge-on objects have lower luminosity and larger line width than the pole-on objects, the putative intermediate objects show the opposite trend – higher luminosity objects have larger line width. The correlation coefficient for these 1081 objects closest to the origin is 0.35, indicating a probability of less than  $10^{-7}$  of no correlation. Thus, our conclusion is that this intermediate subset represents a mix of the low Eddington ratio objects that are pole-on and the high Eddington ratio objects that are edge-on.

### 2.3. Combining the Two Drivers - Orientation and Eddington Ratio

The next step is to divide the intermediate subset into those objects that represent the pole-on counterparts of the edge-on, low Eddington ratio objects and those that represent the edge-on counterparts of the pole-on, high Eddington ratio objects. To do this, note that the solid angle over which objects appear pole-on is smaller than that over which they appear edge-on. Counting objects in the two tails of figure 1 and assuming that these tails represent objects that are within 30 degrees of the preferred orientation, we calculate that approximately half of the intermediate objects should be the edge-on counterparts of the objects that show large [O III] outflows and half should be the pole-on counterparts of the objects that show large Fe II inflows.

Because our interpretation of figure 2 is that the correlation seen between  $L_{5100}$  and FWHM  $H\beta$  is due to the mix of objects with two different sets of physical parameters, we divide the distribution of objects in figure 2 with a line perpendicular to the

best fit line (the bisector of the two dashed lines shown), at a point that divides the distribution into two approximately equal subsets. We choose to label the upper right end of the distribution as the low-Eddington pole-on objects because if the two parts of the intermediate objects were assigned in the opposite sense, they would appear to get brighter when they were viewed edge-on than when they were viewed pole-on. However, both the division and the assignment are speculative and based somewhat on a preconception about the structure and kinematics of the objects in the sample.

### 3. How Some Properties Vary with Orientation and Eddington Ratio

Table 1 gives median properties for the four subsets. All the properties are calculated from data in Table 2 in Hu et al. (2008). Note that the black hole masses are calculated using the values of  $\sigma_{H\beta}$  rather than FWHM  $H\beta$ , and that the Eddington ratios are calculated using  $9\lambda L_{5100}$  as the bolometric luminosity. Uncertainties in these characteristic values for the subsets are in the range of only a few percent, though it should be noted that the range of any property within a subset is large, as can be seen in figure 2. While some quantitative conclusions are drawn below about the behavior of properties within and between subsets, we caution that (a) the subsets are drawn from a parent sample that has been chosen in a way that undoubtedly skews some of these statistics and (b) our definitions of the subsets and how they are associated is arbitrary, though we believe that it all creates a consistent picture. Note particularly that the entire sample is assumed to be the sum of two separable populations, and this is unlikely to be the case. In reality, it is doubtful that a sharp transition exists between objects that show an Fe II inflow if they are seen edge-on and those that show an [O III] outflow if they are seen pole-on. Also, our classification of objects as either edge-on or pole-on certainly weakens the apparent effects.

The behavior of luminosity and broad line width is particularly important as these observables are used to derive black hole mass and Eddington ratio. Both of these properties behave qualitatively as expected given the results of previous studies of the general structure of the BLR

and continuum emitting region. Table 2 shows that  $L_{5100}$  increases as objects are seen more pole-on: by a factor of 2 for high Eddington ratio objects and by a factor of 3 for low Eddington ratio objects.  $H\beta$  width is not strongly dependent on orientation for high Eddington ratio objects, but for low Eddington ratio objects, it is larger by about 15% in those objects seen edge-on.

Consistent with the Risaliti et al. (2011) study,  $EW_{[OIII]}$  is smaller in pole-on objects than in edge-on objects, though the effect is much less than would be expected if [O III] emission were isotropic, and the decrease were due only to the increase in the apparent continuum luminosity. Similarly, the [O III] outflows also seem to broaden the [O III] lines, greatly in the high Eddington ratio objects (by definition), but slightly even in the low Eddington ratio objects, while no such effect is seen in the [O II] lines.

#### 4. Discussion

Overall, a picture consistent with these findings is as follows. The continuum is emitted from the surface of a disk and the BLR is somewhat flattened also. At high ER, both of these regions are less flattened than at low ER. The Fe II inflow, seen in low ER objects, is roughly in the plane of this disk, though it may be that in edge-on objects, we see it at a steep angle, but not zero degrees because of the coplanar obscuring torus. Perpendicular to this disk is the biconical outflow of the narrow forbidden lines. In high ER objects, we see the [O III] coming towards us when our view is pole-on. Lower ionization species probably arise further out where the flow has decelerated.

Estimates of the effect of orientation on  $L_{5100}$  and FWHM  $H\beta$  allow an assessment of its impact on derived quantities  $M_{BH}$  and  $L_{bol}/L_{Edd}$ . Most of the effect appears to be on luminosity, where a factor of 2-3 between edge-on and pole-on objects translates into a shift in both  $M_{BH}$  and ER of 40% to a factor of about 2. The effect on line width, apparently significant only for low Eddington ratio objects, translates into an increase of about 30% in calculated  $M_{BH}$  for edge-on objects, but in the opposite sense to the luminosity effect. It is possible that the line width effect is substantially larger than is seen in this sample, since the objects with very broad  $H\beta$  lines are known to have rela-

tively weak Fe II emission, and so have been preferentially excluded from the Hu et al. (2008) sample. If the quantitative differences between subsets are used to correct each subset to an average orientation, the corrections change the  $M_{BH}$  and  $L_{bol}/L_{Edd}$  numbers by a few tens of percent. They bring the  $M_{BH}$  values closer for similar objects at different orientations. The high and low Eddington ratio subsets retain the same relationship; the high Eddington ratio objects have 2 - 3 times the Eddington ratio value of the low Eddington ratio objects.

This work is a first step towards understanding orientation effects based on the inflow and outflow velocities in large samples. Several questions that represent possible next steps are:

1. For objects without strong Fe II, can the asymmetry of the  $H\beta$  line be used to identify objects that are seen close to edge-on?
2. Can a sufficiently complete and well-defined sample of objects be analyzed in this way to separate orientation-driven and Eddington ratio-driven trends with higher precision?
3. Does a correction to  $M_{BH}$  based on orientation have the effect of reducing the scatter in the  $M_{BH}-\sigma_*$  relation or of clarifying the location of Narrow-Line Seyfert 1s in that diagram?
4. Can trends in other properties, for example, the shape of the  $H\beta$  line, be shown to correlate with orientation, in order to provide additional information about the structure or kinematics of the inner regions of QSOs?

I thank Luigi Foschini and the organizers of the conference *Narrow Line Seyfert 1 Galaxies and Their Place in the Universe*, held in Milan, Italy in April 2011 for the invitation that led to this work. I thank Hermine Landt, Guido Risaliti, and Alessandro Marconi for helpful discussions.

## REFERENCES

- Adelman-McCarthy, J., et al. 2007, ApJS, 172, 634
- Becker, R. H., White, R. L., & Helfand, D. J. 1995, ApJ, 450, 559
- Blandford, R. D. & Konigl, A. 1979, ApJ, 232, 34
- Boroson, T. A. 2005, AJ, 130, 381
- Boroson, T. A., & Green, R. F. 1992, ApJS, 80, 109
- Crenshaw, D. M., Schmidt, H. R., Kraemer, S. B., Mushotzky, R. F., & Dunn, J. P. 2010, ApJ, 708, 419
- Decarli, R., Dotti, M., & Treves, A. 2011, MNRAS, in press
- Gaskell, C. M. 2009, New A Rev., 53, 140
- Hu, C., et al. 2008, ApJ, 687, 78
- Marziani, P., Zamanov, R. K., Sulentic, J. W., & Calvani, M. 2003, MNRAS, 345, 1133
- Richards, G. T. et al. 2002, AJ, 124,1
- Risaliti, G., Salvati, M., & Marconi, A. 2011, MNRAS, 411, 2223
- Ruiz, J. R. et al. 2005, AJ, 129, 73
- Schneider, D. P. et al. 2007, AJ, 134 102
- Urry, C. M. & Padovani, P. 1995, PASP, 107, 803
- Wills, B. J. & Browne, I. W. A. 1986, ApJ, 302, 56
- York, D. G., et al. 2000, AJ, 120, 1579
- Zamanov, R. et al. 2002, ApJ, 576, 9

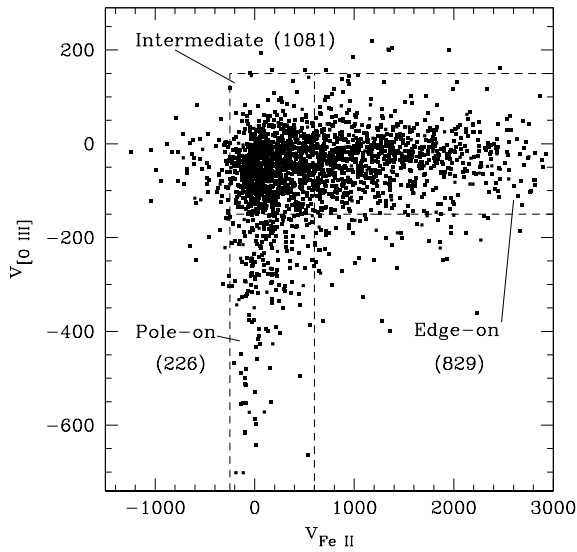


Fig. 1.— The velocity of the [O III]  $\lambda 5007$  line emission plotted against the velocity of the optical Fe II emission, referenced to the systemic redshift, derived from the [O II]  $\lambda 3727$  line. All the velocities are from Hu et al. (2008). The regions marked with dashed lines around the offset velocity tails are assumed to be predominantly edge-on and pole-on objects. The dashed box around the origin designates a set of intermediate objects. The number of objects in each region is indicated.

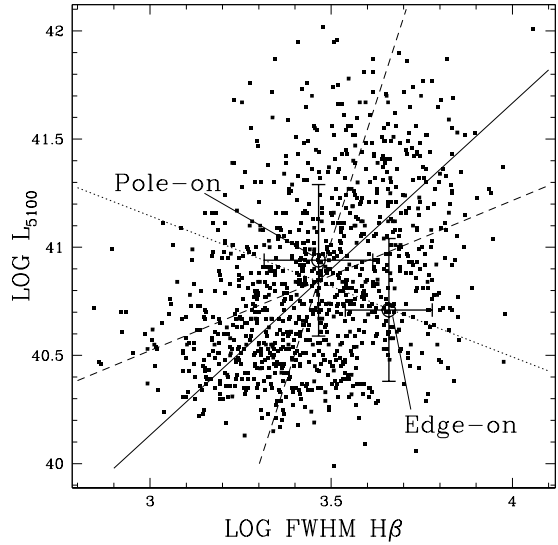


Fig. 2.— Luminosity plotted against  $H\beta$  line width for the objects that show no offset velocity in either Fe II or [O III] and would be intermediate objects if orientation were the only factor. The two large points with error bars show the means and standard deviations for the subsets of objects identified as edge-on or pole-on because of their large offset velocities. The two dashed lines show two least squares fits to the individual points using each of the two variables as the independent variable. The solid line shows the bisector of the two dashed lines. It is clear that the relation between luminosity and line width for the intermediate objects is inconsistent with the trend indicated by the other two subsets, indicating that another factor, Eddington ratio, is important. The dotted line is the adopted dividing line between the two subsets within the part of the sample that shows no offset velocities.

TABLE 1  
MEDIAN PROPERTIES OF SUBSETS

Property	[O III] outflow High Eddington ratio Pole-on	No outflow or inflow High Eddington ratio Edge-on	No outflow or inflow Low Eddington ratio Pole-on	Fe II inflow Low Eddington ratio Edge-on
Number of Objects	226	575	506	829
Log $L_{5100}$ (ergs s <sup>-1</sup> Å <sup>-1</sup> )	40.91	40.56	41.11	40.66
FWHM H $\beta$ (km s <sup>-1</sup> )	2600	2300	3800	4400
EW [O III] (Å)	15.0	16.6	19.6	24.8
EW H $\beta$ (Å)	60	55	73	74
EW Fe II (Å)	55	47	48	37
FWHM [O III] (km s <sup>-1</sup> )	771	405	477	432
FWHM [O II] (km s <sup>-1</sup> )	391	389	438	443
Log $M_{BH}$ ( $M_{\odot}$ )	8.20	7.88	8.59	8.40
$L_{bol}L_{Edd}$ (Eddington Ratio)	0.20	0.19	0.13	0.07